Air Quality, Atmosphere & Health (2022) 15:893–899
https://doi.org/10.1007/s11869-022-01196-x

Transport dynamics of SARS-CoV-2 under outdoor conditions

Mehmet Aydin[1] · Fatih Evrendilek[2] · Ismail Erkan Aydin[3] · Seckin Aydin Savas[4] · Deniz Eren Evrendilek[5]

Received: 1 January 2022 / Accepted: 28 March 2022 / Published online: 2 April 2022

Abstract

This study aimed at estimating the transport dynamics of a single severe acute respiratory syndrome corona-virus 2 (SARS-CoV-2)-laden droplet of 1 to 500 μm in diameter at a wind speed from 1 to 4 m/s. Motion dynamics of SARS-CoV-2-laden respiratory droplets under calm or turbulent air conditions were quantified using a combined model. Dalton's law was implemented to estimate their evaporation. One-factor-at-a-time procedure was applied for the sensitivity analysis of model of deposition velocity. The transport distance of the single virus ranged from 167 to 1120 m as a function of the droplet size, wind speed, and falling time. The evaporation times of the droplets ≤ 3 and ≤ 14 μm in diameter were shorter than their settling times from 1.7 m in height at midnight and midday, respectively. Such droplets remained in the air for about 5 min as the droplet nuclei with SARS-CoV-2. The minimum transport distance of the respiratory droplets of 1–15 μm varied between 8.99 and 142 m at a wind speed range of 1–4 m/s, based on their deposition velocity. With their short transport distance, the larger droplet (30 to 500 μm) was not suspended in the air even under the windy conditions. The deposition velocity was found most sensitive to the droplet diameter. The droplets < 15 μm in diameter completely evaporated at midday and the droplet nuclei with the single virus can travel a minimum distance of 500 m under a horizontal wind speed of 3 m/s.

Keywords COVID-19 · Transport distance · Respiratory droplet size · Droplet evaporation · Dry deposition velocity

Introduction

The globally rapid spread of severe acute respiratory syndrome corona-virus 2 (SARS-CoV-2) and its predictability are of increasingly great concern in terms of devising preventive and mitigative measures (e.g., social distancing) (Sarhan et al. 2021). The first deterministic epidemic model called Susceptible-Infected-Recovered (SIR) was introduced in 1927 and consisted of ordinary differential equations. These deterministic non-linear models of spread and deposition dynamics generate outputs based on parameters and initial condition values (Kermack and McKendrick 1927; Das et al. 2020; Aydin et al. 2021). The motion dynamics of SARS-CoV-2 were quantified in indoor spaces (Anchordoqui and Chudnovsky 2020; Aydin et al. 2021; Sarhan et al. 2021), in the calm air (Aydin et al. 2020a), and under varying outdoor conditions (Das et al. 2020).

The algorithms to solve the spatiotemporal (3D space + time) spread of SARS-CoV-2 can be non-deterministic polynomial-time (NP)-hard in a dynamic environment (e.g., changes in wind speed and direction, solar radiation, temperature, humidity, and population density) according to computational complexity theory (Aydin et al. 2021). The nature of its flow (laminar or turbulent motion) depends upon

✉ Mehmet Aydin
maydin08@yahoo.com

Fatih Evrendilek
fevrendilek@ibu.edu.tr

Ismail Erkan Aydin
erkan.aydin@alanya.edu.tr

Seckin Aydin Savas
seckin.aydin@alanya.edu.tr

Deniz Eren Evrendilek
devrendi@sfu.ca

1 Department of Soil Science (Soil Physics), Mustafa Kemal University, Hatay, Turkey

2 Department of Environmental Engineering, Bolu Abant Izzet Baysal University, Bolu, Turkey

3 Department of Emergency Medicine, Faculty of Medicine, Alanya Alaaddin Keykubat University, Alanya/Antalya, Turkey

4 Department of Plastic and Reconstructive Surgery, Faculty of Medicine, Alanya Alaaddin Keykubat University, Alanya/Antalya, Turkey

5 Department of Computing Science, Simon Fraser University, Burnaby, BC V5A 1S6, Canada

a dimensionless quantity, which is called Reynolds's number (McPherson 1993; Sarhan et al. 2021). In the presence of air resistance, such light objects may perform Brownian motion and follow a pattern of turbulent convective flows, depending on the particle size. In other words, the velocity of the particles at a given point may behave chaotically with time under the turbulent fluctuations (Anchordoqui and Chudnovsky 2020; Chong et al. 2020). Pei et al. (2021) reported that buoyancy-driven flow regime led to a longer transmission distance and elevated exposure to viral aerosols than did the mixing airflow. According to Bond et al. (2021), particle size drives its transport, deposition onto surfaces, and elimination by mitigation measures.

Although recent advances in aerosol instrumentation have enabled numerous deposition measurements (Emerson et al. 2020), the airborne dynamics of SARS-CoV-2 are challenging to model under outdoor conditions. Therefore, a simple approach still remains to be desired to quantify the transport dynamics of SARS-CoV-2 and devise strategies for alleviating the spread of its respiratory droplets. The objective of this study was to quantify the settling and evaporation durations, dry deposition velocity,[1] and minimum transport distance of single SARS-CoV-2-laden respiratory droplets as a function of wind speed (1–4 m/s), vapor pressure deficit (at 22 °C air temperature and 40% relative humidity), and droplet diameter (1–15 and 30–500 μm).

Methods

Motion dynamics of particles under calm air conditions

Aydin et al. (2021) developed a simple model to estimate the terminal/constant velocity of SARS-CoV-2 under the calm indoor or outdoor air conditions. Although the velocity of a falling object is dependent upon the falling time, the predictions of the physical models show a wide variation for the falling time. The velocity of a micro- and/or nano-scale particle may not be constant due to the different particle size, vertical distance, and possible convection of the air. The velocity may be approximated by holding the time constant as follows (Aydin et al. 2021):

$$v_{sm} = \frac{\sqrt{mg}}{2\pi r}\left(\sqrt{\frac{2\pi}{\kappa\rho_a}} + \frac{\sqrt{mg}}{6\eta}\right)(1 - 1/e) \quad (1)$$

where v_{sm} is the effective speed of motion (m/s); m is the particle mass (kg); g is the gravitational acceleration (9.81 m/s^2); π is 3.1416; r is the particle radius (m); κ is a shape-dependent coefficient such as 0.47 for water droplets of a spherical shape which was assumed as 1.99 for a single isolated SARS-CoV-2 due to its spikes; ρ_a is the air density (1.2041 kg/m^3 at 20 °C and 1 atm); η is the dynamical viscosity of air [1.85×10^{-5} kg/(m s)]; and e is a mathematical constant (the base of natural logarithm also known as Euler's number: ~ 2.718). The SARS-CoV-2 was assumed as a single particle of a spherical shape with an average diameter of 100 nanometer (nm) and a protein density of 1.35×10^3 kg/m^3. Thus, the volume and mass of a single virus were estimated at 5.236×10^{-22} m^3 and 7.07×10^{-19} kg, respectively (Aydin et al. 2020a, 2021). The cross-surface area of a single virus is assumed to equal the surface area of a hemisphere $\left(2\pi r^2\right)$ where the base is not included, due to the wing area of its spikes. Thus, the expression of $\sqrt{2\pi/\kappa\rho_a}$ in Eq. (1) can be parameterized as $\sqrt{\pi/\kappa\rho_a}$ for a single SARS-CoV-2. The falling (settling) time (t) of a single SARS-CoV-2 from a given height (z) in the calm indoor air whether it is encapsulated by a droplet or not can be quantified thus (Aydin et al. 2021):

$$t = z/v_{sm} \quad (2)$$

Motion dynamics of particles under turbulent air conditions

Turbulence necessitates detailed physical analysis since the interactions within turbulence create a complex (chaotic) flow pattern that changes with time and space. Under the windy conditions, the interactions among SARS-CoV-2, respiratory droplets, and dust particles may occur. The transport distance of the atmospheric particles depends on flow conditions and particle size. Shao (2008) established an approximate relationship between particle size and transport distance under specific atmospheric conditions:

$$x_d = W_s z/v_d \quad (3)$$

where x_d is particle travel distance (m); W_s is wind speed (m/s); z is height from the ground surface (m); and v_d is dry deposition velocity (m/s). Though generally calculated as a function of particle flux and concentration, the deposition velocity can be obtained as follows (Giardina and Buffa 2018):

$$v_d = \frac{v_{sm}}{1 - e^{-[r_z v_{sm}]}} \quad (4)$$

where r_z is the total resistance (s/m) to transport as a function of particle diameter (d) and height (Z) (Giardina and Buffa 2018; Aydin et al. 2021). In the above equation, we

[1] The dry deposition is the free fall of particles from the atmosphere onto Earth where deposition occurs without precipitation.

used v_{sm} as the settling velocity (m/s) of the particle. The total resistance (r_z) can be determined as follows (Giardina and Buffa 2018):

$$r_z = r_a + r_{ql} \tag{5}$$

where r_a is an aerodynamic resistance (s/m); and r_{ql} is a quasi-laminar sub-layer (boundary layer) resistance (s/m). The phenomena associated with the boundary layer effects are influenced by Reynolds's number and surface roughness. Re-entrainment can be analyzed considering the drag and frictional forces on the particles on or very close to the solid surfaces (McPherson 1993). The aerodynamic resistance can be determined using the Monin–Obukhov similarity theory (Giardina and Buffa 2018):

$$r_a = \left(1\mathrm{n}\left(z/z_0\right) - \varphi\right)/ku^* \tag{6}$$

where z_0 is the surface roughness height above the displacement plane; k is the von Karman constant (0.4); and u^* is the friction velocity, the intensity of the atmospheric turbulence. The parameter φ in Eq. (6) can be calculated according to Brandt et al. (2002):

$$\varphi = -5\frac{z}{L}, with\ \frac{z}{L} > 0\ (stable\ atmospheric\ conditions) \tag{7}$$

and

$$\varphi = e^{\left\{0.598+0.390ln\left(-\frac{z}{L}\right)-0.09\left[ln\left(-\frac{z}{L}\right)\right]^2\right.}, \quad with\ \frac{z}{L} < 0\ (unstable\ atmospheric\ conditions) \tag{8}$$

where L is Monin–Obukhov length which was set as 125 m and − 150 m for stable and unstable air conditions, respectively (Sathe et al. 2010). To facilitate a comparison, we have selected the same reference height (z) of 1.7 m, an average human height. The boundary-layer resistance can be estimated thus (UK Met Office Hadley Centre 2017):

$$r_{ql} = \left(S_c/P_r\right)^{2/3}/ku^* \tag{9}$$

where S_c is the Schmidt number (diffusion vs viscosity); and P_r is the Prandtl number of 0.72 for the lower atmosphere (Liu et al. 1979; UK Met Office Hadley Centre 2017). At 20 °C in the ambient atmosphere, the Schmidt number was assumed as 1.28 (Wu et al. 1992). u^* was assumed as 0.114 m/s for smooth grounds in Eqs. (6) and (9) (Giardina and Buffa 2018). The assumed relationship in Eq. (9) is an over-simplification. The deposition speed was modeled for the stable and unstable air conditions, based on a single SARS-CoV-2 particle (protein) density of 1.35×10^3 kg/m^3, a respiratory water droplet density of 998 kg/m^3, and a roughness length (z_0) of 0.02 m (Giardina and Buffa 2018; Aydin et al. 2020a).

Evaporation of respiratory droplets

The droplets are subject to evaporation once coming out of the respiratory tract. The further the droplets are away from the mouth, the smaller the droplet size is due to evaporation (Anchordoqui and Chudnovsky 2020; Stariolo 2020). Aydin et al. (2021) approximated droplet evaporation as a function of air temperature and relative humidity for indoor conditions thus:

$$E_{di} = 4\left(0.364\ exp\ \left(0.084T_a\right) + 3.64\ exp\ (-0.021RH)\right) \tag{10}$$

where E_{di} is indoor droplet evaporation (mm/day); T_a is daily mean value of air temperature in the range of 2–49 °C; and RH is relative humidity in the range of 10–90%. Solar radiation, wind speed, temperature, and relative humidity are the primary climatic drivers of the outdoor evaporation (Allen et al. 1994; Aydin 2008; Aydin et al. 2020b). If pan-evaporation data are not available, then outside water evaporation can be computed via the simplest and most common type of Dalton's law as follows (Helfrich et al. 1982):

$$E_{po} = u\left(e_s - e_a\right) \tag{11}$$

where E_{po} is outdoor pan evaporation (mm/day); e_s is saturated water vapor pressure (mm of mercury); e_a is actual vapor pressure in the air (mm of mercury); and u is a function of wind speed. Saturated vapor pressure (mbar) can be expressed thus (1 mbar = 0.75 mm of mercury) (Allen et al. 1994):

$$e_s = 6.1078\ exp\ \left(17.2694 \times T_a/\left(T_a + 237.3\right)\right) \tag{12}$$

e_a (mbar) can be estimated as follows (Allen et al. 1994):

$$e_a = RH \times e_s/100 \tag{13}$$

u can be estimated thus (Helfrich et al. 1982):

$$u = a + b \times W_s \tag{14}$$

where W_s is wind speed (m/s) at a height of 2.0 m (hereafter u_2); a and b are constants. To estimate the parameter of u, the daily constants ($a = 0.675$, $b = 0.142$, with u_2 expressed in m/s) were derived from the data by Malek (1994) and Srivastava and Jain (2017).

In this study, droplet evaporation was adjusted by considering the effects of the surface area exposed to the atmospheric evaporative demand but by neglecting the collective influence of a typical cloud of droplets, based on Aydin et al. (2021). Therefore, outdoor droplet evaporation (E_{do}, mm/day) can be derived thus:

$$E_{do} = 4\left(u\left(e_s - e_a\right)\right) \tag{15}$$

Sensitivity analysis

Sensitivity analysis conducted in this study helped to identify the important model parameters, test the model conceptualization, and improve the model structure (Sieber and Uhlenbrook 2005; Aydin and Kececioglu 2010). Therefore, the sensitivity of the dry deposition velocity (v_d) in Eq. (4) to the droplet size (d or 2r), the friction velocity (u^*), Schmidt number (S_c), and Monin–Obukhov length (L) was determined (see Eq. 1 and from Eqs. 5, 6, 7, 8 and 9). In so doing, one-factor-at-a-time procedure was applied through which a given predictor was changed by a predetermined fractional increase and decrease in several steps, while keeping the others at their nominal values. Thus, their sensitivities were detected by monitoring the corresponding changes in the output relative to the baselines.

Results and discussion

The transport distances of an isolated single SARS-CoV-2 are presented as a function of wind speed in Fig. 1. Its dry deposition velocity was firstly derived from Eq. (4) as deposition is a process by which atmospheric particles are removed by a turbulent transfer and fall onto the earth's surface. Equation (4) may yield irrational results for the airborne nano-scale particles with a high density (such as a protein density of 1.35×10^3 kg/m^3), while Eq. (3) underestimates the transport distances considerably. Therefore, the transport distance of a single SARS-CoV-2 was estimated by using both v_{sm} and v_d for a comparison and ranged from 281 and 167 m at a wind speed of 1 m/s to 1120 and 667 m at a wind speed of 4 m/s, respectively (Fig. 1). The atmospheric lifetime of the virus was not considered in Fig. 1.

As a one-way flux, the deposition velocity of a single SARS-CoV-2-laden respiratory droplet is shown in Fig. 2. Its velocity exhibited an asymptotic exponential growth with its rising droplet diameter. The dry deposition velocity of the respiratory droplet from 1.7 m in height varied between 0.05 m/s for a diameter of 1 µm and 0.19 m/s for a diameter of 15 µm. Evaporation time of a single SARS-CoV-2-laden respiratory droplet is illustrated in Fig. 3, together with its settling time. On a diurnal average, the falling time of a respiratory droplet > 7 µm from 1.7 m was shorter than its evaporation time. In other words, the droplets larger than 7 µm settled faster than they evaporated, whereas the smaller droplets evaporated faster than they settled down. Similar findings were reported by Bourouiba (2020) and Wells (1934). However, Anchordoqui and Chudnovsky (2020) reported very short evaporation times for the wide range of droplet sizes of 50 to 2000 µm. According to Aydin et al. (2021), the atmospheric evaporative demand, aka vapor pressure deficit, increased as the day progressed and peaked ten times faster at midday than midnight based on hourly percentages of daily evaporation data. In this study, the approach suggested by Aydin et al. (2021) was implemented to calculate hourly percentages of daily evaporation. According to their approach, the droplets with the diameters ≤ 3 and ≤ 14 µm were capable of the complete evaporation and remained in the air for about 4.7 min as the droplet nuclei with SARS-CoV-2 at midnight and midday, respectively. The detailed theoretical discussions of the evaporation of aqueous droplets in a rapidly changing outdoor condition were made by Abramzon and Sirignano (1989). Our simulations were independent of the host-dependent survival duration of

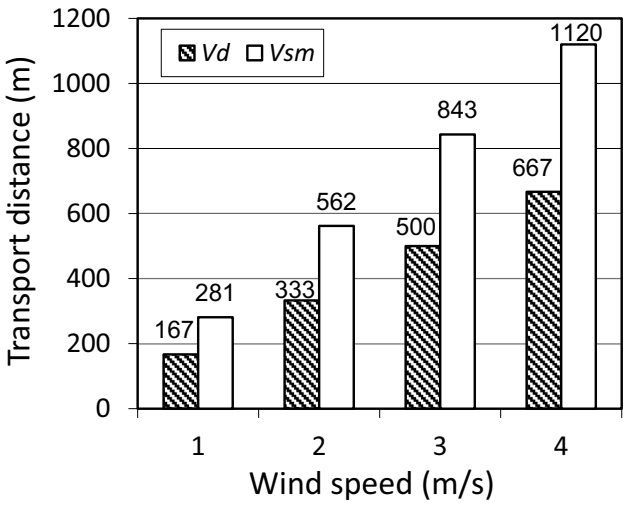

Fig. 1 Transport distance of a single SARS-CoV-2 from 1.7 m in height as a function of wind speed based on Eq. (3) using deposition (v_d) and settling (v_{sm}) velocities

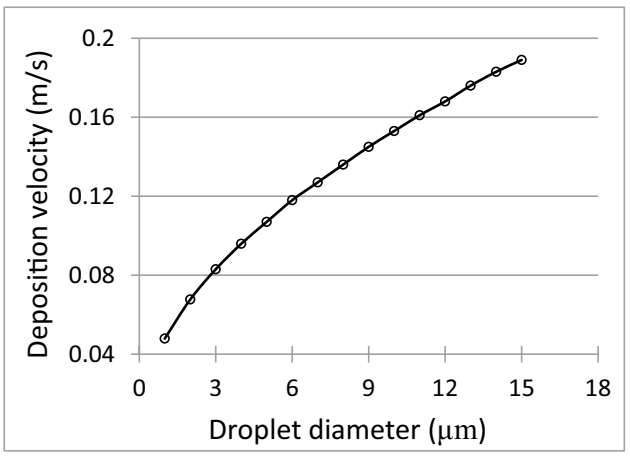

Fig. 2 Dry deposition velocity of a single SARS-CoV-2-laden respiratory droplet based on Eq. (4)

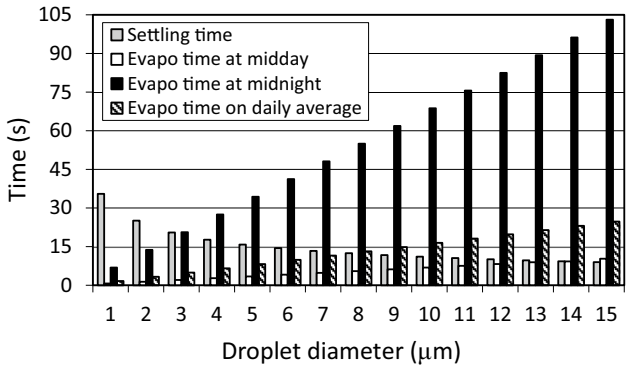

Fig. 3 Settling and evaporation (evapo) durations of a single SARS-CoV-2-laden respiratory droplet as a function of its diameter and daytime versus nighttime at a wind speed of 3 m/s

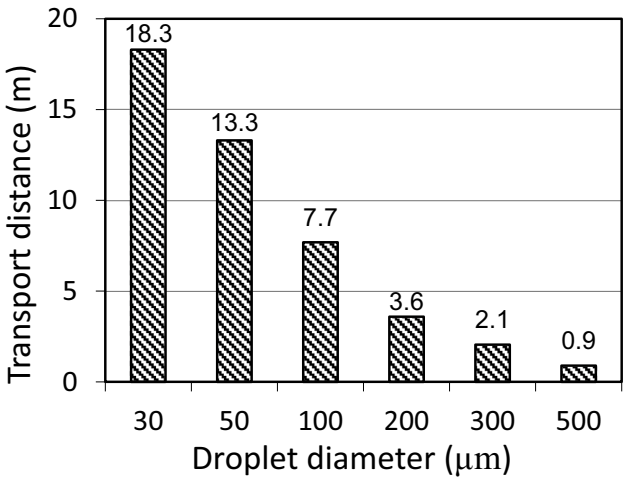

Fig. 5 Minimum transport distance of a single SARS-CoV-2-laden respiratory droplet from 1.7 m in height as a function of a large diameter at a wind speed of 3 m/s

SARS-CoV-2 suspended in the air and the possible influence of a typical cloud of droplets.

According to Fig. 4, the minimum transport distance of a single SARS-CoV-2-laden respiratory droplet with a diameter of 1 μm from 1.7 m in height was estimated at 142 m under a wind speed of 4 m/s. However, its evaporation can cause the virus to have a longer transport distance and time in the air since it reduces the droplet diameter (Bathula et al. 2021). As can be seen in Fig. 5, the minimum transport distance of the larger droplets (30 to 500 μm) under a wind speed of 3 m/s was very short. Since the settling times of the larger droplets were shorter than their evaporation times, they were not suspended in the air even under the windy conditions. According to Sarhan et al. (2021), most of the respiratory droplets similarly fell onto the floor due to gravity before travelling 1.5 m in an indoor environment where the airborne transmission of the virus was ignored. Feng et al. (2020) reported that high relative humidity expanded the droplet diameter which in turn increased the deposition fractions, while, with the complex wind and humidity conditions, micro-droplets were influenced by convection and transported from the human coughs/sneezes to other humans in less than 5 s. Likewise, at very low wind speeds, convection was reported to significantly induce the mixing at the reference height, while wind perturbations exerted a more surface stress than did the average wind (Bourassa et al. 1999). According to Kayalar et al. (2021), temperature, wind speed, relative humidity, and precipitation significantly influence the vitality and transmission of biological constituents of aerosols characterized by the suitability and atmospheric lifetime/travel distance of suspended particles. Hadei et al. (2021) concluded that air pollution can exacerbate COVID-19-related incidences and mortality.

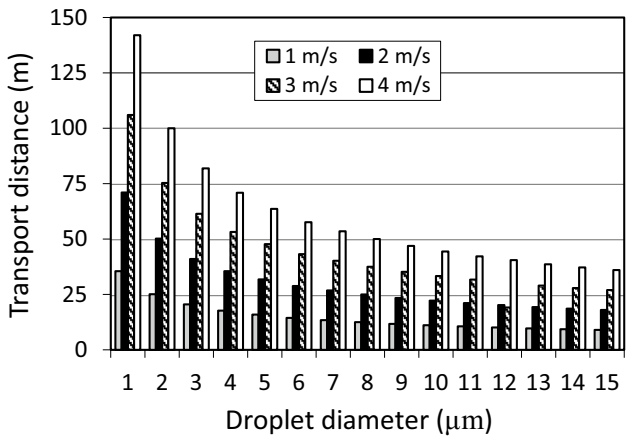

Fig. 4 Minimum transport distance of a single SARS-CoV-2-laden respiratory droplet from 1.7 m in height as a function of diameter and wind speed

The dry deposition velocity was most sensitive to the droplet diameter. The droplet mass and diameter were assumed to be parallel. Friction velocity was rated as the second most effective variable, whereas the contributions of Monin–Obukhov length and Schmidt number to the response were negligible (Table 1). According to Aydin et al. (2015), the sensitivity outcomes may not reflect the site-specific conditions.

Our striking findings are illustrated in Fig. 6. The droplets ≥ 15 μm settled down at the end of their transport distances. The droplets < 15 μm in diameter completely evaporated at midday and traveled as far as the single virus went. In other words, the droplets < 15 μm evaporated completely within their transport distances, while the droplet nuclei with the single virus traveled at least 500 m under a horizontal wind speed of 3 m/s. These results may be of interest to the environmental and/or public health communities.

Table 1 Sensitivity of the dry deposition velocity to several predictors

x: Percent change in predictor	*y*: Percent change in dry deposition velocity (*Vd*)	R^2 (%)	*n*	Percent change in predictor	Percent change in *Vd*
Droplet diameter, *2r*	$y = 0.533x$	99.06	11	100	53.3
Friction velocity, *u**	$y = 10^{-4}x^2 + 0.052x - 0.8$	99.82	6	100	5.4
Schmidt number, *Sc*	$y = 2\ ^{x}\ 10^{-5}x^2$-$0.0024x - 0.0041$	99.43	5	100	−0.0441
Monin–Obukhov length, *L*	$y = -10^{-7}x^2 + 0.0002x + 0.0124$	93.15	6	100	0.0314

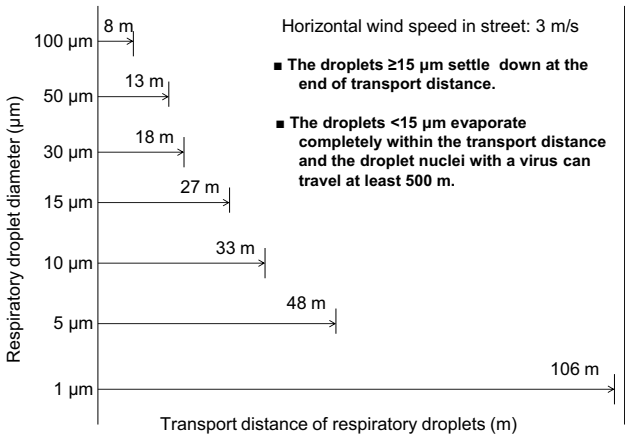

Fig. 6 Transport distance of a single SARS-CoV-2-laden respiratory droplet as a function of its diameter

Conclusions

The suggested approach in this study contributes to the better quantification of the transport dynamics of SARS-CoV-2. The transport distance of a single virus showed a wide range of 167 to 1120 m as a function of the droplet size, wind speed, and falling time. The dry deposition velocities of the respiratory droplets increased with their diameters. In other words, the deposition velocity was most sensitive to the droplet diameter and least sensitive to Monin–Obukhov length and Schmidt number. The droplets larger than 7 µm settled down faster than they evaporated based on a daily evaporation rate. The droplets ≤ 14 µm were able to evaporate completely and remained in the air for about 5 min as droplet nuclei with SARS-CoV-2 at midday. The nuclei of these droplets with the single virus traveled at least 500 m under a horizontal wind speed of 3 m/s. Model validations and further experimental observations still remain to be desired to measure and enhance the predictive power.

Author contribution Mehmet Aydin, Fatih Evrendilek, and Ismail Erkan Aydin carried out the conceptualization and design of the study as well as the drafting and editing of the manuscript. Seckin Aydin Savas and Deniz Eren Evrendilek carried out the acquisition, analysis, simulation, and interpretation of data. All the authors reviewed the manuscript.

Data availability Data will be made available on request. Correspondence and requests for materials should be addressed to Mehmet Aydin.

Declarations

Competing interests The authors declare no competing interests.

References

Abramzon B, Sirignano WA (1989) Droplet vaporization model for spray combustion calculations. Int J Heat Mass Transfer 32(9):1605–1618. https://doi.org/10.1016/0017-9310(89)90043-4

Allen RG, Smith M, Perrier A, Pereira LS (1994) An update for the definition of reference evapotranspiration. ICID Bull 43(2):92

Anchordoqui LA, Chudnovsky EM (2020) A physicist view of COVID-19 airborne infection through convective airflow in indoor spaces. Sci Med J 2:68–72. https://doi.org/10.28991/SciMedJ-2020-02-SI-5

Aydin M (2008) A model for evaporation and drainage investigations at ground of ordinary rainfed-areas. Ecol Model 217(1–2):148–156. https://doi.org/10.1016/j.ecolmodel.2008.06.015

Aydin M, Kececioglu SF (2010) Sensitivity analysis of evaporation module of E-DiGOR model. Turk J Agric for 34(6):497–507. https://doi.org/10.3906/tar-0909-398

Aydin M, Jung Y-S, Yang JE, Kim S-J, Kim K-D (2015) Sensitivity of soil evaporation and reference evapotranspiration to climatic variables in South Korea. Turk J Agric for 39(6):652–662. https://doi.org/10.3906/tar-1406-170

Aydin M, Evrendilek F, Savas SA, Aydin IE, Evrendilek DE (2020a) Falling dynamics of SARS-CoV-2 as a function of respiratory droplet size and human height. J Med Biol Eng 40:880–886. https://doi.org/10.1007/s40846-020-00575-y

Aydin M, Aydin B, Polat V (2020b) Modeling and computer simulation of Drainage, Evaporation, and Runoff (DEaR) from bare soils. Fresenius Environ Bull 29(04A):3287–3299

Aydin M, Savas SA, Evrendilek F, Aydin IE, Evrendilek DE (2021) A model for indoor motion dynamics of SARS-CoV-2 as a function of respiratory droplet size and evaporation. Environ Monit Assess 193(10):626

Bathula S, Anand S, Thajudeen T, Mayya YS, Chaudhury P, Shashank C (2021) Survival of expiratory aerosols in a room: study using a bi-compartment and bi-component indoor air model. Aerosol Air Qual Res 21(5):200547. https://doi.org/10.4209/aaqr.200547

Bond TC, Bosco-Lauth A, Farmer DK, Francisco PW, Pierce JR, Fedak KM, Ham JM, Jathar SH, Woude SV (2021) Quantifying proximity, confinement, and interventions in disease outbreaks: a

decision support framework for air-transported pathogens. Environ Sci Technol 55:2890–2898. https://doi.org/10.1021/acs.est.0c07721

Bourassa MA, Vincent DG, Wood WL (1999) A flux parameterization including the effects of capillary waves and sea state. J Atmos Sci 56:1123–1139

Bourouiba L (2020) Turbulent gas clouds and respiratory pathogen emissions: potential implications for reducing transmission of COVID-19. JAMA 323(18):1837–1838. https://jamanetwork.com/on04/08/2021

Brandt J, Christensen JH, Frohn LM (2002) Modelling transport and deposition of caesium and iodine from the Chernobyl accident using the DREAM model. Atmos Chem Phys 2:397–417. https://doi.org/10.5194/acp-2-397-2002

Chong KL, Shi J-Q, Ding G-Y, Ding S-S, Lu H-Y, Zhong J-Q, Xia K-Q (2020) Vortices as Brownian particles in turbulent flows. Sci Adv 6(34):eaaz1110. https://doi.org/10.1126/sciadv.aaz1110

Das SK, Alam J, Plumari S, Greco V (2020) Transmission of airborne virus through sneezed and coughed droplets. Phys Fluids 32:097102. https://doi.org/10.1063/5.0022859

Emersona EW, Hodshire AL, DeBolt HM, Bilsback KR, Pierce JR, McMeeking GR, Farmer DK (2020) Revisiting particle dry deposition and its role in radiative effect estimates. PNAS 117(42):26076–26082. https://www.pnas.org/cgi/doi/https://doi.org/10.1073/pnas.2014761117.

Feng Y, Marchal T, Sperry T, Yi H (2020) Influence of wind and relative humidity on the social distancing effectiveness to prevent COVID-19 airborne transmission: A numerical study. J Aerosol Sci 147:105585. https://doi.org/10.1016/j.jaerosci.2020.105585

Giardina M, Buffa P (2018) A new approach for modeling dry deposition velocity of particles. Atmos Environ 180:11–22. https://doi.org/10.1016/j.atmosenv.2018.02.038

Hadei M, Hopke PK, Shahsavani A, Raeisi A, Jafari AJ et al (2021) Effect of short-term exposure to air pollution on COVID-19 mortality and morbidity in Iranian cities. J Environ Health Sci Eng 19:1807–1816. https://doi.org/10.1007/s40201-021-00736-4

Helfrich KR, Adams EE, Godbey AL, Harleman DRF (1982) Evaluation of models for predicting evaporative water loss in cooling impoundments. Massachusetts Institute of Technology, Energy Laboratory Report No. MIT-EL 82–017:164 pp.

Kayalar O, Ari A, Babuccu G, Konyalilar N, Dogan O et al (2021) Existence of SARS-CoV-2 RNA on ambient particulate matter samples: a nationwide study in Turkey. Sci Total Environ 789:147976. https://doi.org/10.1016/j.scitotenv.2021.147976

Kermack WO, McKendrick AG (1927) A contribution to the mathematical theory of epidemics. Proc R Soc London a: Math Phys Eng Sci 115:700–721

Liu WT, Katsaros KB, Businger JA (1979) Bulk parameterization of air–sea exchanges of heat and water vapor including the molecular constraints at the interface. J Atmos Sci 36:1722–1735

Malek E (1994) Calibration of the Penman wind function using the Bowen ratio energy balance method. J Hydrol 163(3–4):289–298. https://doi.org/10.1016/0022-1694(94)90145-7

McPherson MJ (1993) The Aerodynamics, Sources and Control of Airborne Dust. Chapter 20:1–40.

Pei G, Taylor M, Rim D (2021) Human exposure to respiratory aerosols in a ventilated room: Effects of ventilation condition, emission mode, and social distancing. Sustain Cities Soc 73:103090. https://doi.org/10.1016/j.scs.2021.103090

Sarhan AR, Naser P, Naser J (2021) COVID-19 aerodynamic evaluation of social distancing in indoor environments, a numerical study. J Environ Health Sci Eng 19:1969–1978. https://doi.org/10.1007/s40201-021-00748-0

Sathe A, Mann J, Gottschall J, Courtney MS (2010) Estimating the systematic errors in turbulence sensed by wind lidars. Risø National Laboratory, Roskilde, Denmark. Risø–R–1759(EN). Pitney Bowes Management Services Denmark A/S. 24 pp.

Shao Y (2008) Physics and Modelling of Wind Erosion, 2 edn., Springer-Berlin, 420 pp.

Sieber A, Uhlenbrook S (2005) Sensitivity analyses of a distributed catchment model to verify the model structure. J Hydrol 310:216–235

Srivastava R, Jain A (2017) Engineering Hydrology. McGraw-Hill Education, India. e-Edition-ISBN: 9352606213, 9789352606214.

Stariolo DA (2020) COVID-19 in air suspensions. *arXiv*:2004.05699v2.

UK Met Office Hadley Centre (2017) Dry deposition in UKCA –what is it? How does it work? UKCA Training Workshop –Cambridge, 9–13 January, 2017.

Wells WF (1934) On air-borne infection: study II. droplets and droplet nuclei. Am J Epidemiol 20:611–618. https://doi.org/10.1093/oxfordjournals.aje.a118097

Wu Y-L, Davidson CI, Dolske DA, Sherwood SI (1992) Dry deposition of atmospheric contaminants: the relative importance of aerodynamic, boundary layer, and surface resistances. Aerosol Sci Technol 16:65–81